ACS APPLIED MATERIALS & INTERFACES

Research Article

www.acsami.org

CVD Graphene as Interfacial Layer to Engineer the Organic Donor–Acceptor Heterojunction Interface Properties

Shu Zhong,[†] Jian Qiang Zhong,[‡] Hong Ying Mao,[†] Rui Wang,[‡] Yu Wang,[†] Dong Chen Qi,[‡] Kian Ping Loh,[†] Andrew Thye Shen Wee,[‡] Zhi Kuan Chen,[†,§] and Wei Chen*[,†,‡]

[†]Department of Chemistry, National University of Singapore, 3 Science Drive 3, Singapore 117543

[‡]Department of Physics, National University of Singapore, 3 Science Drive 2, Singapore 117542

[§]Institute of Materials Research & Engineering, 3 Research Link, 117602, Singapore

Supporting Information

ABSTRACT: We demonstrate the use of chemical-vapor-deposited (CVD) graphene as an effective indium–tin-oxide (ITO) electrode surface modifier to engineer the organic donor–acceptor heterojunction interface properties in an inverted organic solar cell device configuration. As revealed by in situ near-edge X-ray adsorption fine structure measurement, the organic donor–acceptor heterojunction, comprising copper-hexadecafluoro-phthalocyanine (F_{16}CuPc) and copper phthalocyanine (CuPc), undergoes an obvious orientation transition from a standing configuration (molecular π-plane nearly perpendicular to the substrate surface) on the bare ITO electrode to a less standing configuration with the molecular π-plane stacking adopting a large projection along the direction perpendicular to the electrode surface on the CVD graphene-modified ITO electrode. Such templated less-standing configuration of the organic heterojunction could significantly enhance the efficiency of charge transport along the direction perpendicular to the electrode surface in the planar heterojunction-based devices. Compared with the typical standing organic–organic heterojunction on the bare ITO electrode, our in situ ultraviolet photoelectron spectroscopy experiments reveal that the heterojunction on the CVD graphene modified ITO electrode possesses better aligned energy levels with respective electrodes, hence facilitating effective charge collection.

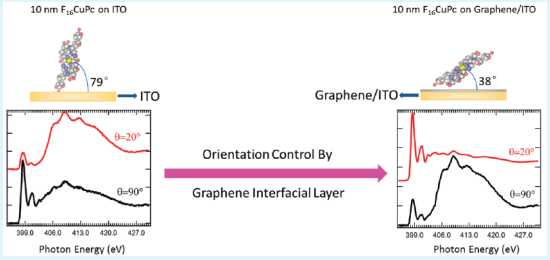

KEYWORDS: *graphene, interfacial layer, electrode modification, organic heterojunction, molecular orientation, energy level alignment*

INTRODUCTION

Graphene has been widely used in organic optoelectronic devices in the past few years because of its outstanding electronic transport and optical properties, excellent structural flexibility, chemical stability, and ease of chemical functionalization.[1−6] In the field of organic photovoltaic (OPV) cells, examples include the use of reduced graphene oxide (rGO) and chemical-vapor-deposited (CVD) graphene as transparent electrode to replace indium tin oxide (ITO),[7−10] the use of graphene or graphene derivatives as the active layers to generate light-induced charge carriers,[11,12] or the use of graphene oxide (GO) as the anode buffer layer to replace or dope PEDOT:PSS, and hence to help transport holes and block electrons.[7,13] It has also been reported that the solution-processed graphene or graphene composite can be used as the anode in organic light-emitting diodes.[14,15] For the application in organic field-effect-transistors (OFETs), due to the structural similarity between the graphene and the π-conjugated organic molecules such as pentacene, CVD graphene has been used to effectively modify the source and drain electrodes to form better electrical contacts with pentacene.[16,17] The anode interfacial layers in OPV cells are usually high work function materials, like PEDOT:PSS (5.2 eV),[18] MoO_3 (6.8 eV)[19] and V_2O_5 (7.0 eV).[20] They can form better contact with the donor material with reduced hole injection barrier.[21] Although the low work function of graphene of about 4.2–4.5 eV[1,6,9,11,22,23] prohibits its use as the anode buffer layer, it is desirable to be used at the cathode side. Recently, inverted solar cells have achieved reasonably good power conversion efficiency,[18] better device stability, longer lifetime and the ease of integration with solution processing.[18,24−26] In the normal device configuration of OPVs, metals with low work function are required to match the lowest-unoccupied-molecular-orbital (LUMO) of the acceptor-type organic semiconductors. They are not very stable as the top electrodes due to the sensitivity to oxygen and moisture in air. The inverted OPV structure can circumvent this drawback by using high work function metals like silver or gold as the top anode with much better stability.[27] Therefore, it is ideal to use CVD graphene as the cathode buffer layer in an inverted solar cell to satisfy the considerations of both the device stability and the low work function of the graphene.

Received: March 16, 2012
Accepted: May 24, 2012
Published: June 4, 2012

We recently reported the use of CVD graphene as an effective structural template to control the interfacial molecular orientation of chloroaluminium phthalocyanine (ClAlPc), making the ClAlPc molecules lie flat on the CVD graphene modified ITO electrode compared to the random orientations on the bare ITO.[22] The lying ClAlPc molecules with their π-plane stacking direction nearly perpendicular to the ITO surface could improve the efficiency of charge transport along this direction in an OPV device. In the present study, we demonstrate that the CVD graphene film can also be used as an effective ITO electrode modifier to engineer the interface properties of organic donor−acceptor heterojunctions. Copper-hexadecafluoro-phthalocyanine (F_{16}CuPc) has been chosen as the acceptor material to integrate with the common p-type semiconductor copper phthalocyanine (CuPc) to form OOHs. F_{16}CuPc is an attractive alternative to the conventionally used C_{60} in small-molecule-based OPV cells because of the broad light absorption (550−850 nm), high electron mobility (0.02−0.6 $cm^2\ V^{-1}\ s^{-1}$), and excellent stability in air.[28] The orientation and interfacial electronic structure of the OOHs on the CVD graphene modified ITO and bare ITO were studied by near-edge X-ray absorption fine structure (NEXAFS) and ultraviolet photoelectron spectroscopy (UPS) measurements, respectively. In contrast to the standing configuration on the bare ITO, the heterojunction compromising F_{16}CuPc and CuPc adopts a less-standing configuration on the CVD graphene-modified ITO electrode. Such templated less standing configuration of the F_{16}CuPc/CuPc OOH results in a larger projection of the π-stacking direction along the transport direction in a typical planar heterojunction-based device, and hence could significantly enhance the charge transport efficiency along this direction. Moreover, the better aligned energy levels of the heterojunction on CVD graphene-modified ITO electrode also facilitate effective charge injection or collection.

EXPERIMENTAL METHODS

Monolayer graphene films were synthesized via the CVD process on thermally annealed copper foil. To transfer the graphene films, normal wet-transfer technology based on polymethylmethacrylate (PMMA) was used. After etching the copper foil with $FeCl_3$ and HCl solution, the graphene film with the PMMA support was transferred to the clean ITO substrate.[9,23] ITO glass substrates without patterned (for NEXAFS and UPS measurements) or with patterned (for device fabrication) were cleaned by successive sonication in a detergent (Hellmanex) bath, deionized water, acetone and isopropanol, and blow-dried under N_2. The substrates were baked in an oven at 80 °C before use.

The molecular orientation of organic films on both the CVD graphene-modified ITO electrode and the bare ITO electrode was probed by angular-dependent NEXAFS measurement. NEXAFS spectra of N K-edge were recorded in Auger electron yield (AEY) mode for thin F_{16}CuPc (0.5 nm) on graphene/ITO and total electron yield (TEY) mode for all other thick films at the SINS beamline of the Singapore Synchrotron Light Source using 97% linearly polarized synchrotron light.[29,30] The N K-edge NEXAFS spectra in AEY acquisition mode are collected by measuring the N *KLL* Auger electrons centered at 377 eV with a 16 eV energy integration window. The interfacial electronic structures of the ITO/F_{16}CuPc/CuPc and ITO/graphene/F_{16}CuPc/CuPc were monitored by in situ UPS measurements in a customer-built ultrahigh vacuum (UHV) system. All UPS spectra were recorded at normal emission angle, and the secondary electron cutoff was measured with −5 V sample bias. The work function of the substrate ϕ was obtained through the equation $\phi = h\nu - W$, where W is the spectrum width of the energy difference between substrate Fermi level and secondary electron cutoff. Before deposition, the CVD graphene modified ITO substrate was degassed at 300 °C in the ultrahigh vacuum preparation chamber with pressure below 1×10^{-8} Torr overnight to get rid of PMMA residual. Sublimation purified F_{16}CuPc and CuPc were evaporated in situ from two separate Kundsen cells onto the substrate. During the growth, the sample was held at room temperature (RT) and the deposition rate was 0.2 nm/min, calibrated by a quartz-crystal-microbalance (QCM).

For the device fabrication, the F_{16}CuPc, CuPc, MoO_3 and Ag layers were sequentially thermally evaporated (1.2 nm/min for organic molecules, 0.6 nm/min for MoO_3 and 6.0 nm/min for Ag) in the vacuum chamber with a base pressure of $\sim 10^{-7}$ mbar. The active area of the device was 0.09 mm^2. The thickness of the films were measured by QCM and further calibrated by a surface profiler. Current density−voltage (J−V) measurements were carried out in an inert environment (Braun glovebox, N_2 atmosphere) under 1 sun (AM 1.5G) conditions using a solar simulator with a light intensity of 100 mW/cm^2.

RESULTS AND DISCUSSION

Figure 1b shows the angle-dependent N K-edge NEXAFS spectra for 10 nm F_{16}CuPc on the bare ITO. The first three

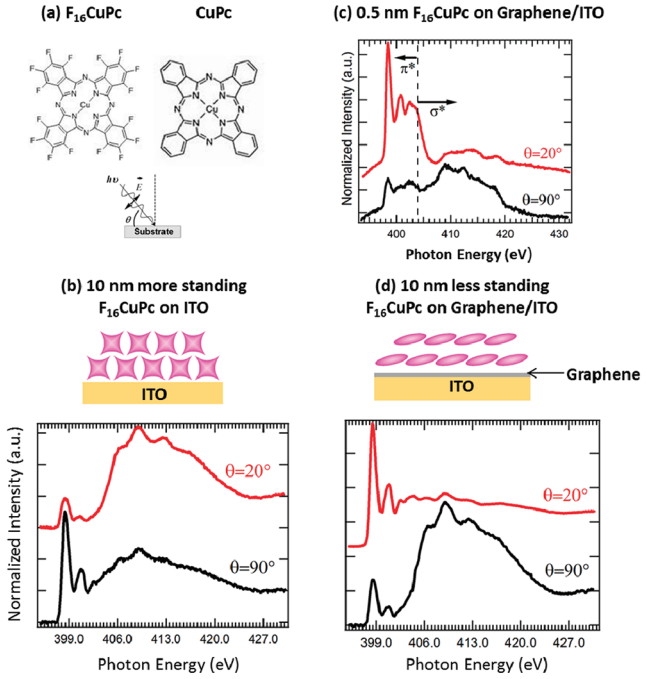

Figure 1. (a) Schematic drawing showing the molecular structures of F_{16}CuPc and CuPc. Angle-dependent N-edge NEXAFS spectra for (b) 10 nm F_{16}CuPc on the bare ITO, (c) 0.5 nm, and (d) 10 nm F_{16}CuPc on the graphene-modified ITO.

absorption peaks (397−405 eV) arise from the resonant transitions from the N 1s core level into different π^* orbitals of F_{16}CuPc. The broad absorption peaks at higher photon energies (405−420 eV) are the transitions to the σ^* states.[31] For the disk-shaped F_{16}CuPc, the π^* orbitals orient essentially perpendicular to the molecular plane and the σ^* orbitals in the molecular plane.[31] As shown in Figure 1b, the intensity of the π^* absorption peaks of F_{16}CuPc is suppressed at grazing incidence (θ = 20°) and greatly enhanced at normal incidence (θ = 90°). This indicates that the F_{16}CuPc molecules adopt a standing configuration with their molecular π-plane oriented nearly perpendicular to the substrate surface. The intensity I of the π^* resonance is related to the tilt angle α of the F_{16}CuPc molecular plane with respect to the substrate plane and the synchrotron light incidence angle θ by[32]

dx.doi.org/10.1021/am300887j | ACS Appl. Mater. Interfaces 2012, 4, 3134−3140

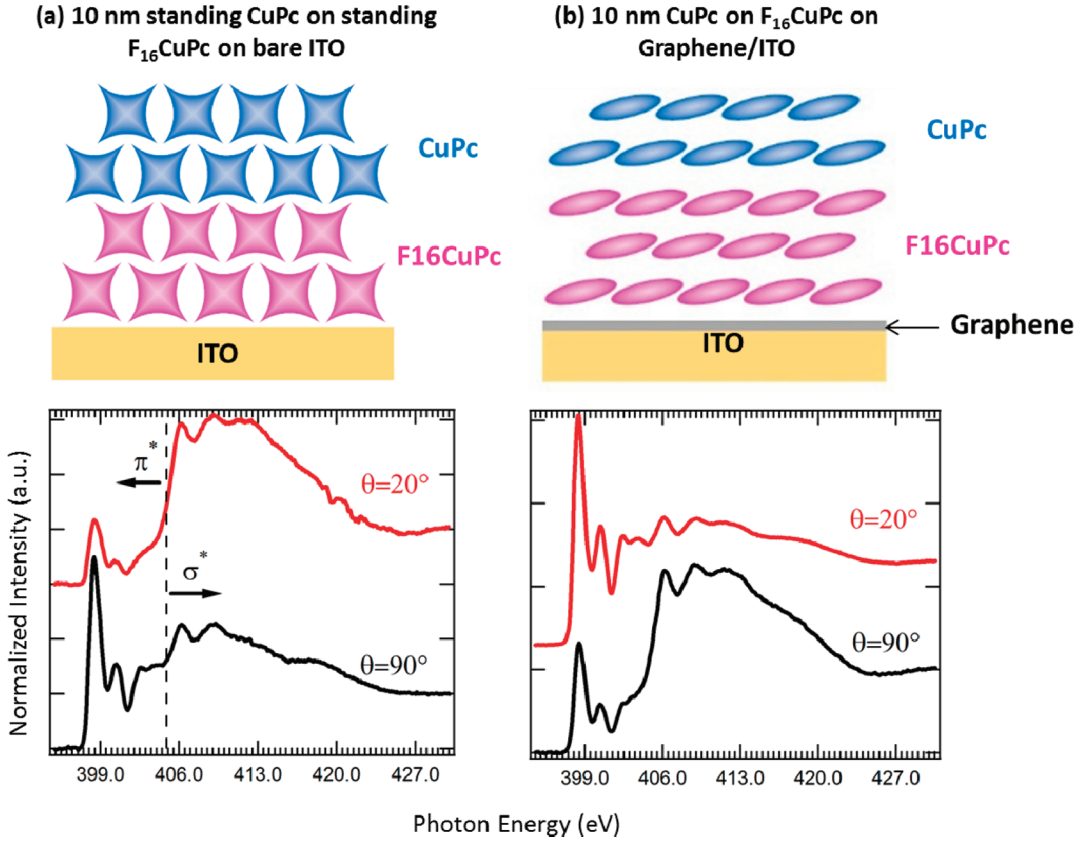

Figure 2. Angle-dependent N K-edge NEXAFS spectra for 10 nm CuPc on 10 nm F_{16}CuPc on (a) the bare ITO and (b) the graphene-modified ITO.

$$I(\theta) \infty 1 + \frac{1}{2}(3\cos^2\theta - 1)(3\cos^2\alpha - 1)$$

Using the intensity ration R (π^*) = $I(90°)/I(20°)$, we can estimate the average tilt angle for 10 nm F_{16}CuPc is 79° ± 5°. In contrast, as shown in panels c and d in Figure 1, the π^* resonance of F_{16}CuPc on the graphene-modified ITO substrate is greatly enhanced at grazing incidence but largely depressed at normal incidence. The tilt angle is estimated to be 34° ± 5° for 0.5 nm F_{16}CuPc on graphene-modified ITO substrate, showing that the F_{16}CuPc molecules adopt almost lying configuration with their molecular π-plane stacking having a large projection along the direction perpendicular to the substrate surface. The thicker 10 nm F_{16}CuPc film on grapheme also has a similar orientation with an average tilt angle α = 38° ± 5°.

Such templating effect on the molecular orientation of organic films can be even reflected on the top organic layer in an OOH using the CVD graphene-modified ITO electrode. As shown in Figure 2a, after the further deposition of 10 nm CuPc on 10 nm F_{16}CuPc film on the bare ITO electrode, CuPc molecules still adopt an apparently standing configuration on the standing F_{16}CuPc film with the tilt angle estimated to be 74° ± 5°, as revealed by the angle-dependent NEXAFS measurement.[31] On the other hand, CuPc molecules show less standing configuration with the tilt angle estimated to be 42° ± 5° on the F_{16}CuPc film on the CVD grapheme modified ITO (Figure 2b). Because of the interfacial π–π interaction, F_{16}CuPc molecules orient with their stacked molecular π-plane possessing a large projection along the surface normal on the CVD graphene modified ITO electrode. The exposed molecular π-plane of the less standing F_{16}CuPc molecules can be further used as a structural template to engineer the molecular orientation of the CuPc film deposited on top, arising from the intermolecular π–π interaction. It has been previously reported that a lying F_{16}CuPc/CuPc heterojunction can be grown on the bulk graphite substrate, arising from the directional interfacial π–π interactions between the π electrons in graphite and those in F_{16}CuPc and CuPc.[33] Our present study confirms that even the monolayer graphene can realize the same structural templating effect in controlling the molecular orientation in organic donor–acceptor heterojunctions. With such less-standing configuration of the F_{16}CuPc/CuPc heterojunction on the CVD graphene-modified ITO substrate, the π-plane stacking direction of the molecules has larger projection along the direction normal to the substrate surface, as compared with the standing OOH on the bare ITO. When operated in an OPV device, the molecular π-plane stacking direction is essentially oriented closer to the charge transport direction, hence facilitating the efficient charge transport in the organic heterojunction fabricated on the CVD graphene-modified ITO electrode.

The molecular orientation strongly affects the energy-level alignment at OOH interfaces.[31,33−35] To evaluate the energy level alignment at the F_{16}CuPc/CuPc heterojunction interface on the CVD graphene-modified ITO substrate, we carried out in situ UPS measurements. For comparison, we first investigated the energy level alignment of the standing F_{16}CuPc/CuPc heterojunction on the bare ITO substrate. Figure 3 shows the evolution of the thickness-dependent UPS spectra for 10 nm CuPc on 10 nm F_{16}CuPc on the bare ITO. As displayed in Figure 3a, the vacuum level shifts to the higher kinetic energy gradually by 1.48 ± 0.02 eV with the increase of

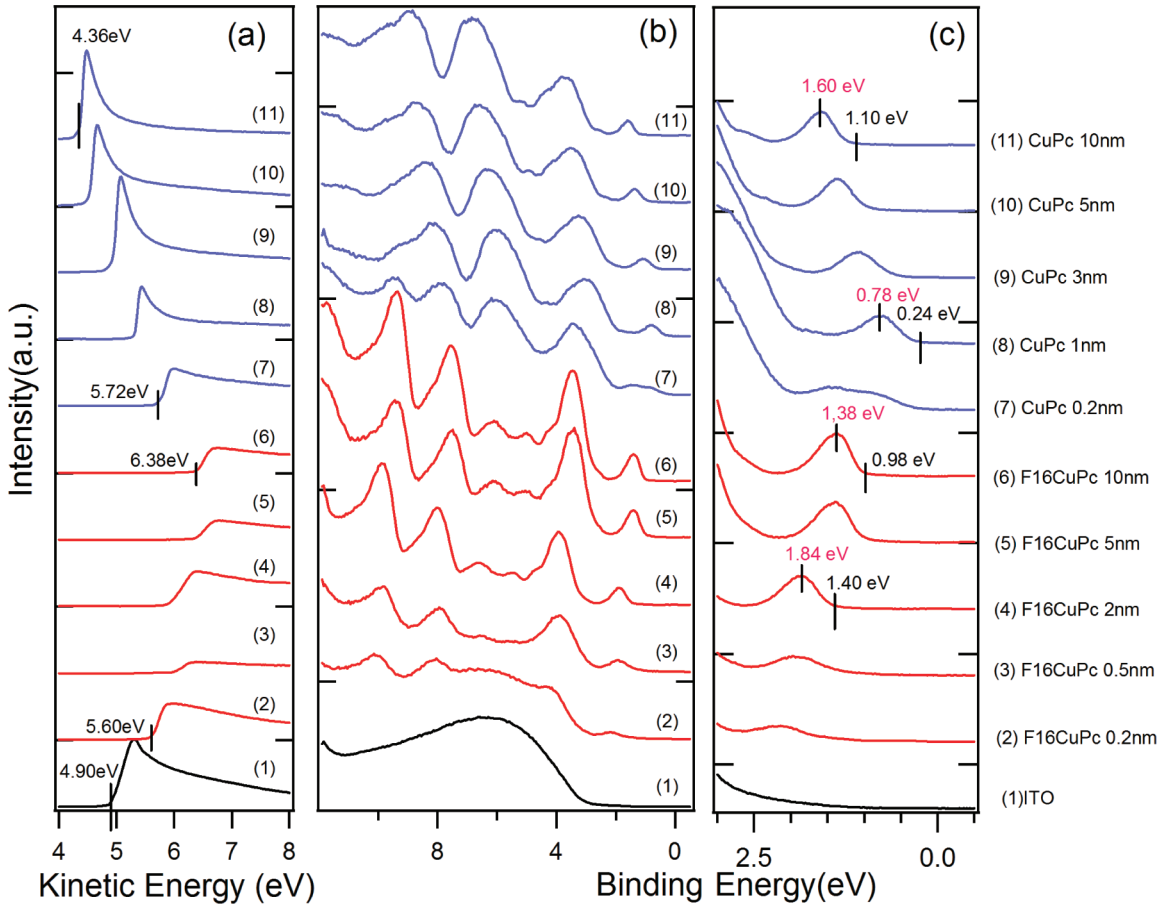

Figure 3. UPS spectra at (a) the low kinetic energy region (secondary electron cutoff), (b) the low binding energy region (the valence band region), and (c) the corresponding valence band region near the Fermi level during the sequential deposition of 10 nm CuPc on 10 nm F_{16}CuPc on the bare ITO.

the thickness of F_{16}CuPc film, in another words, the work function is gradually increased by 1.48 ± 0.02 eV after the growth of 10 nm F_{16}CuPc on bare ITO. At the same time, the highest-occupied-molecular-orbital (HOMO) leading edge of F_{16}CuPc moves toward lower binding energy and finally locates at 0.98 ± 0.02 eV. After further deposition of CuPc molecules, a downward shift of the vacuum level by 2.02 ± 0.02 eV was observed, or the work function was decreased by 2.02 ± 0.02 eV after growing 10 nm CuPc. Meanwhile, the HOMO leading edge of the CuPc film gradually moves to the higher binding energy and finally locates at 1.10 ± 0.02 eV. This indicates a significant charge transfer has occurred at the F_{16}CuPc/CuPc heterojunction interface fabricated on the bare ITO.

In contrast, the degree of the charge transfer at the F_{16}CuPc/CuPc heterojunction interface grown on the CVD graphene modified ITO is much smaller compared with that on bare ITO. As shown in panels a and c in Figure 4, after the deposition of 10 nm F_{16}CuPc on the CVD graphene-modified ITO, the HOMO leading edge is almost aligned at 1.32 ± 0.02 eV, associated with a rather small upward vacuum level shift of about 0.76 ± 0.02 eV. As shown in Figure 4c, after the sequential deposition of CuPc on the F_{16}CuPc on CVD graphene modified ITO, the CuPc HOMO leading edge gradually moves to the higher binding energy and finally locates at 0.67 ± 0.02 eV for 10 nm CuPc on 10 nm F_{16}CuPc. It is worth highlighting that the vacuum level downward shift at this F_{16}CuPc/CuPc heterojunction interface is measured to be about 1.02 ± 0.02 eV, much smaller compared with that grown on the bare ITO. This indicates that a much weaker charge transfer occurs at the F_{16}CuPc/CuPc heterojunction interface grown on the CVD graphene-modified ITO.

The energy level diagrams of the two systems are illustrated in Figure 5. The HOMO positions are derived from the UPS measurements. The transport band gap (HOMO−LUMO gap) and hence the LUMO positions are taken from previously reported inverse photoemission spectroscopy (IPES) measurements.[36] Clearly, we can observe a much larger vacuum level shift or change in work function at the standing F_{16}CuPc/CuPc heterojunction interface fabricated on the bare ITO compared with that at the less standing F_{16}CuPc/CuPc heterojunction interface on the CVD graphene-modified ITO. This is accompanied by a larger HOMO onset shift and interfacial charge transfer for the standing OOH on the bare ITO, as can been in Figure 5a. Because the charge transfer at the standing CuPc/F_{16}CuPc interface is very strong, the Fermi level is first pinned at the HOMO edge after the depletion of all the gap states at the low thickness region of CuPc. Further increasing the thickness of the CuPc leads to the Fermi level moving into the HOMO−LUMO gap and pinned at the gap states above the HOMO due to the weaker charge transfer away from the interface.[37] In particular, the large charge transfer at the standing OOH interface grown on bare ITO results in the formation of an electron accumulation layer in the n-type F_{16}CuPc layer and a hole accumulation layer in the p-type CuPc layer, i.e., the formation of an accumulation-type OOH. This could serve as an additional energy barrier for electrons

dx.doi.org/10.1021/am300887j | ACS Appl. Mater. Interfaces 2012, 4, 3134−3140

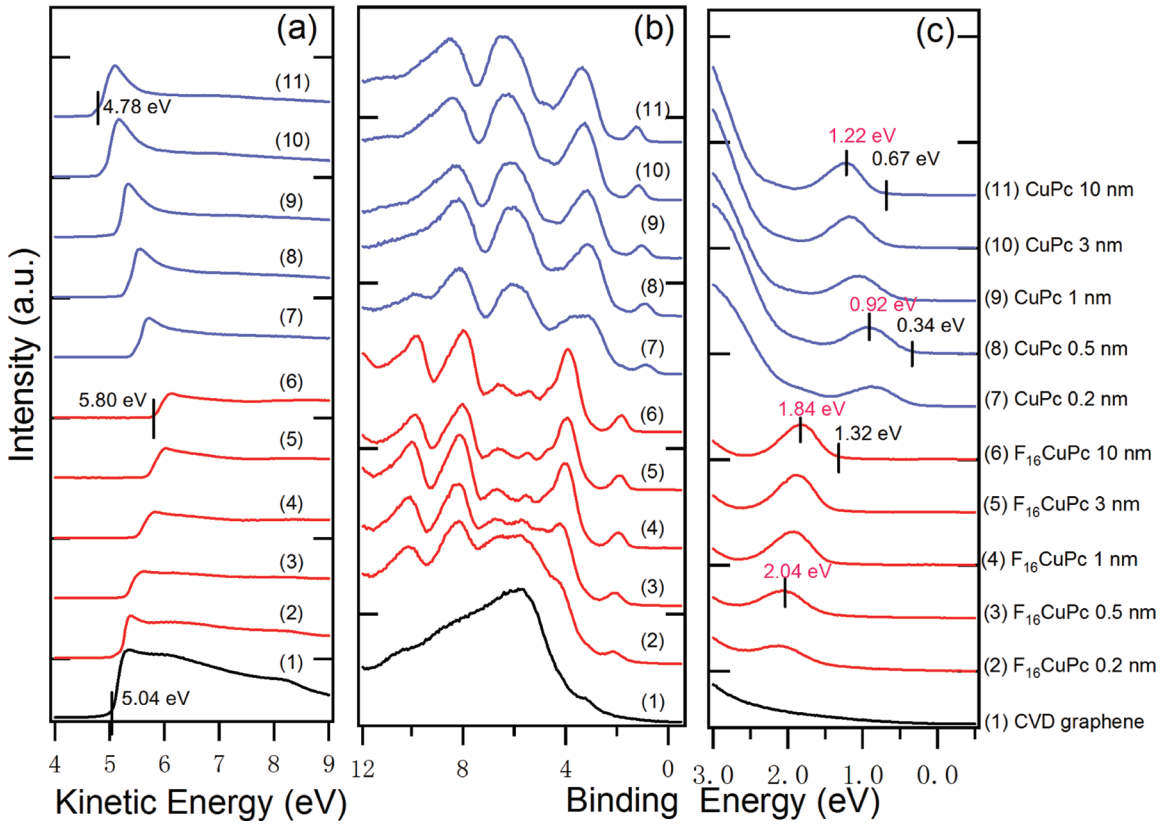

Figure 4. UPS spectra at (a) the low kinetic energy region (secondary electron cutoff), (b) the low binding energy region (the valence band region), and (c) the corresponding valence band region near the Fermi level during the sequential deposition of 10 nm CuPc on 10 nm F_{16}CuPc on the CVD graphene-modified ITO.

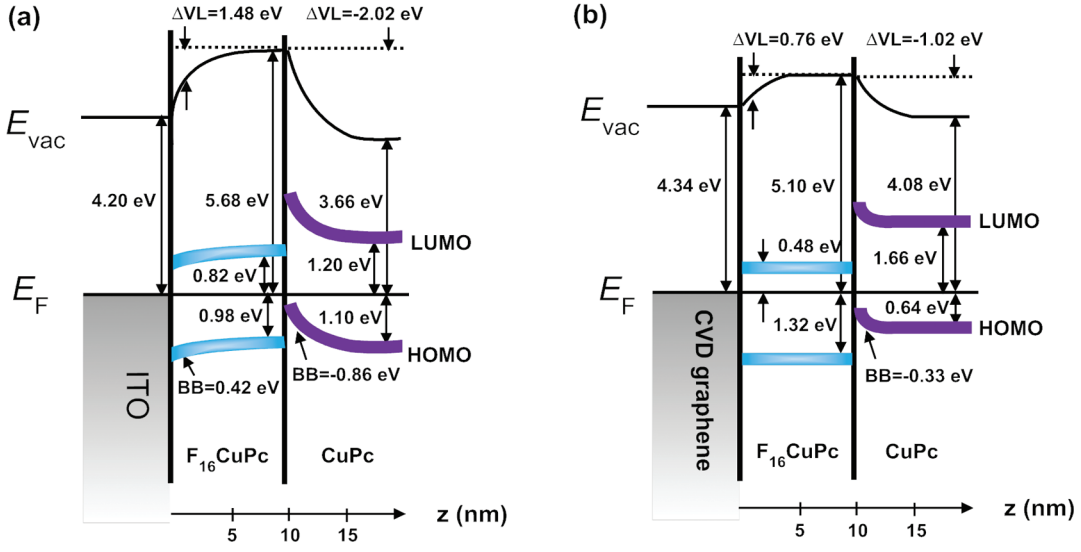

Figure 5. Schematic energy level diagrams of (a) the standing CuPc film on the standing F_{16}CuPc film on the bare ITO and (b) the less standing CuPc film on the less standing F_{16}CuPc film on the CVD graphene modified ITO.

(holes) transferring to the n (p)-type organic semiconductor under light illumination. The charge accumulation in the standing accumulation-type OOH may prohibit effective light-induced charge separation at the donor−acceptor interface, thereby leading to low power conversion efficiency.[31,37−41] Such undesirable effect can be minimized in some extent by growing the less standing OOHs on the CVD graphene modified ITO. As shown in Figure 5b, the charge transfer at the lying F_{16}CuPc/CuPc interface is much weaker, as indicated by the much smaller vacuum level shift and the change of the hole injection barrier measured to be 1.02 ± 0.02 and 0.33 ± 0.02 eV, respectively. By using the CVD graphene modified ITO as cathode in an inverted OPV cell, because of the small work function of graphene (~4.34 ± 0.02 eV in this work), a reasonable small electron injection barrier between the F_{16}CuPc LUMO and the Fermi level is estimated to be around

dx.doi.org/10.1021/am300887j | ACS Appl. Mater. Interfaces 2012, 4, 3134−3140

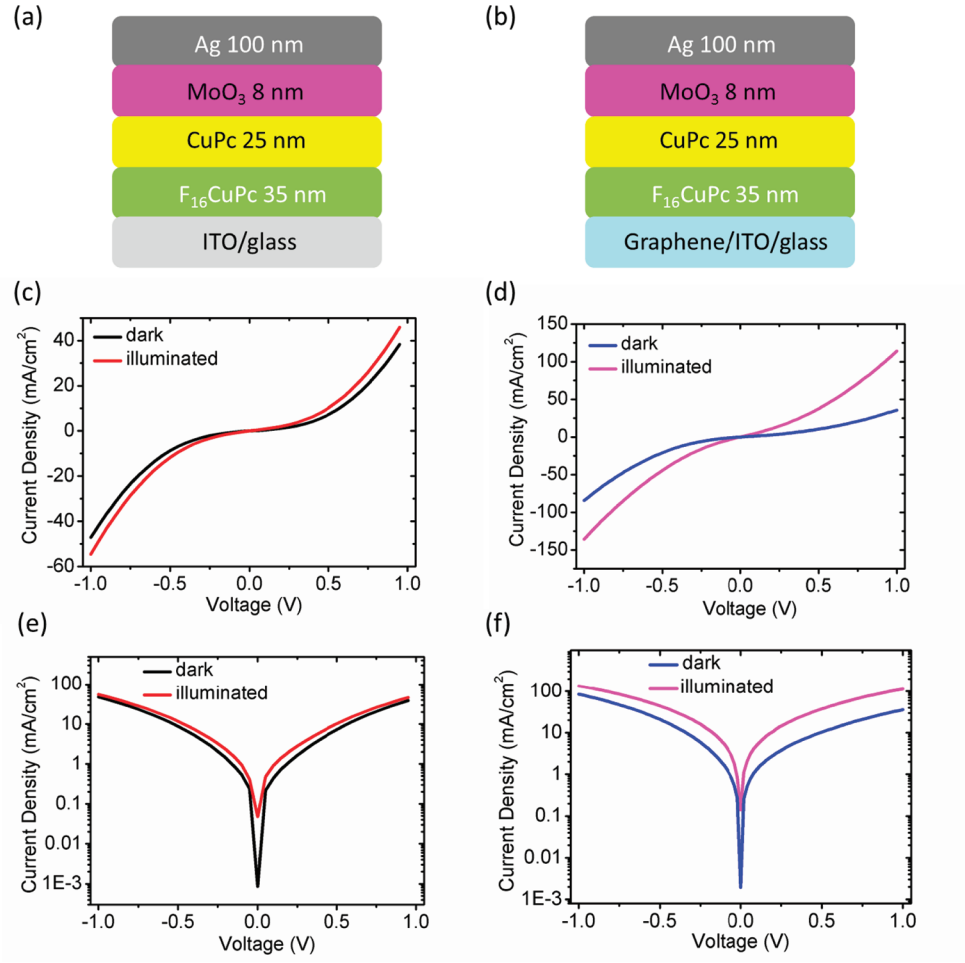

Figure 6. Schematic illustration of the device structure (a) ITO/F_{16}CuPc (35 nm)/CuPc (25 nm)/MoO_3 (8 nm)/Ag (100 nm) and (b) ITO/CVD graphene/F_{16}CuPc (35 nm)/CuPc (25 nm)/MoO_3 (8 nm)/Ag (100 nm). Linear scale current density vs voltage (J–V) curves for the device (c) without or (d) with graphene. Log scale current density vs voltage (J–V) curves for the device (e) without or (f) with graphene.

0.48 ± 0.02 eV, indicating its potential use in inverted OPVs. The morphologies of the F_{16}CuPc/CuPc heterojunction on both substrates can be found in the Supporting Information.

To evaluate the effect of the interfacial graphene layer on the organic heterojunction properties, we fabricated the F_{16}CuPc/CuPc heterojunction based model devices on the bare ITO and the graphene modified ITO. The device structures and J–V curves with linear scale and log scale under dark and simulated AM 1.5G light illumination are illustrated in Figure 6. As shown in panels c and e in Figure 6, the device on the bare ITO possesses a very conducting characteristic with large dark current and no apparent diode property. As revealed by our interface investigation, a strong interfacial charge transfer and large band-bending occur at the F_{16}CuPc/CuPc heterojunction interface on the bare ITO, and hence the formation of accumulation type heterojunction. This could lead to the observed highly conducting nature of the standing F_{16}CuPc/CuPc heterojunction on the bare ITO under dark, consistent with previous reports,[42−46] demonstrating their potential uses as charge generation layer in tandem organic light-emitting diodes or the interconnection layer in the tandem OPVs.[47,48] In particular, as shown in panels c and e in Figure 6, light illumination does not induce an apparent conductance enhancement. The standing F_{16}CuPc/CuPc heterojunction on the bare ITO is highly self-doped because of the strong interfacial charge transfer. The light illumination induced charge carriers could not significantly increase the charge carrier concentration of this heterojunction, and thereby there is no obvious light induced conductivity enhancement. In contrast, for the device on the CVD graphene modified ITO (Figure 6d, f), the light -induced photocurrent in the forward bias condition was about 1 order of magnitude higher as compared to the dark current. The graphene interfacial layer can modulate the molecular orientation of the F_{16}CuPc thin films from the standing configuration on the bare ITO with the tilt angle of 79° ± 5° to the less-standing configuration with the tilt angle of 38° ± 5°. This results in a significantly reduced degree of charge transfer at the F_{16}CuPc/CuPc heterojunction interfaces, and hence largely decreases the interfacial charge transfer induced charge carrier concentration of the heterojunction on the graphene-modified ITO. Light illumination on this less-doped heterojunction could effectively increase the charge carrier concentration, and hence the observation of the obvious light induced conductivity enhancement. Although the F_{16}CuPc/CuPc is not an ideal donor−acceptor system for OPV devices, it clearly demonstrates the effect of the graphene layer to engineer the organic heterojunction interface properties.

CONCLUSION

CVD graphene has been demonstrated as an effective ITO electrode modifier to manipulate the molecular orientation of

the F_{16}CuPc/CuPc OOH, resulting in a transition from the standing OOH on the bare ITO to a less standing OOH with the molecular π-plane stacking adopting a large projection along the charge transport direction (i.e., perpendicular to the electrode surface). The less-standing configuration in OOH could improve the efficiency of charge transport when operated in planar heterojunction-based device. As demonstrated by in situ UPS measurements, the low work function of CVD graphene leads to a small electron injection barrier between the n-type F_{16}CuPc with large electron affinity and the CVD graphene-modified ITO cathode, facilitating its use in inverted OPV cells.

■ ASSOCIATED CONTENT

Supporting Information

Morphologies of the organic films on ITO and graphene-modified ITO. This material is available free of charge via the Internet at http://pubs.acs.org.

■ AUTHOR INFORMATION

Corresponding Author

*E-mail: phycw@nus.edu.sg.

Notes

The authors declare no competing financial interest.

■ ACKNOWLEDGMENTS

The authors acknowledge the support from the Singapore ARF Grant R143-000-440-112, NUS YIA Grant R143-000-452-101, NUS FRC-SPORE program, and NRF-CRP Grant "Graphene and Related Materials and Devices".

■ REFERENCES

(1) Bonaccorso, F.; Sun, Z.; Hasan, T.; Ferrari, A. C. *Nat. Photonics* **2010**, *4*, 611−622.
(2) Pang, S. P.; Tsao, H. N.; Feng, X. L.; Mullen, K. *Adv. Mater.* **2009**, *21*, 3488−3491.
(3) Liu, W.; Jackson, B. L.; Zhu, J.; Miao, C. Q.; Chung, C. H.; Park, Y. J.; Sun, K.; Woo, J.; Xie, Y. H. *ACS Nano* **2010**, *4*, 3927−3932.
(4) Kim, K. S.; Zhao, Y.; Jang, H.; Lee, S. Y.; Kim, J. M.; Ahn, J. H.; Kim, P.; Choi, J. Y.; Hong, B. H. *Nature* **2009**, *457*, 706−710.
(5) Lee, W. H.; Park, J.; Sim, S. H.; Jo, S. B.; Kim, K. S.; Hong, B. H.; Cho, K. *Adv. Mater.* **2011**, *23*, 1752−1756.
(6) Wang, X.; Zhi, L. J.; Mullen, K. *Nano Lett.* **2008**, *8*, 323−327.
(7) Wan, X.; Long, G.; Huang, L.; Chen, Y. *Adv. Mater.* **2011**, *23*, 5342−5358.
(8) De Arco, L. G.; Zhang, Y.; Schlenker, C. W.; Ryu, K.; Thompson, M. E.; Zhou, C. W. *Acs Nano* **2010**, *4*, 2865−2873.
(9) Wang, Y.; Tong, S. W.; Xu, X. F.; Ozyilmaz, B.; Loh, K. P. *Adv. Mater.* **2011**, *23*, 1514−1518.
(10) Wu, J. B.; Becerril, H. A.; Bao, Z. N.; Liu, Z. F.; Chen, Y. S.; Peumans, P. *Appl. Phys. Lett.* **2008**, *92*, 263302.
(11) Liu, Z. F.; Liu, Q.; Huang, Y.; Ma, Y. F.; Yin, S. G.; Zhang, X. Y.; Sun, W.; Chen, Y. S. *Adv. Mater.* **2008**, *20*, 3924−3930.
(12) Li, Y.; Hu, Y.; Zhao, Y.; Shi, G. Q.; Deng, L. E.; Hou, Y. B.; Qu, L. T. *Adv. Mater.* **2011**, *23*, 776−780.
(13) Li, S. S.; Tu, K. H.; Lin, C. C.; Chen, C. W.; Chhowalla, M. *ACS Nano* **2010**, *4*, 3169−3174.
(14) Wu, J. B.; Agrawal, M.; Becerril, H. A.; Bao, Z. N.; Liu, Z. F.; Chen, Y. S.; Peumans, P. *ACS Nano* **2010**, *4*, 43−48.
(15) Chang, H. X.; Wang, G. F.; Yang, A.; Tao, X. M.; Liu, X. Q.; Shen, Y. D.; Zheng, Z. J. *Adv. Funct. Mater.* **2010**, *20*, 2893−2902.
(16) Di, C. A.; Wei, D. C.; Yu, G.; Liu, Y. Q.; Guo, Y. L.; Zhu, D. B. *Adv. Mater.* **2008**, *20*, 3289−3293.
(17) Lee, W. H.; Park, J.; Sim, S. H.; Lim, S.; Kim, K. S.; Hong, B. H.; Cho, K. *J. Am. Chem. Soc.* **2011**, *133*, 4447−4454.
(18) Chen, C. P.; Chen, Y. D.; Chuang, S. C. *Adv. Mater.* **2011**, *23*, 3859−3863.
(19) Xie, L. F.; Wang, X.; Mao, H. Y.; Wang, R.; Ding, M. Z.; Wang, Y.; Ozyilmaz, B.; Loh, K. P.; Wee, A. T. S.; Ariando; Chen, W. *Appl. Phys. Lett.* **2011**, *99*, 012112.
(20) Meyer, J.; Zilberberg, K.; Riedl, T.; Kahn, A. *J. Appl. Phys.* **2011**, *110*, 033710.
(21) Chen, L. M.; Xu, Z.; Hong, Z. R.; Yang, Y. *J. Mater. Chem.* **2010**, *20*, 10947−10947.
(22) Mao, H. Y.; Wang, R.; Wang, Y.; Niu, T. C.; Zhong, J. Q.; Huang, M. Y.; Qi, D. C.; Loh, K. P.; Wee, A. T. S.; Chen, W. *Appl. Phys. Lett.* **2011**, *99*, 093301.
(23) Wang, Y.; Chen, X. H.; Zhong, Y. L.; Zhu, F. R.; Loh, K. P. *Appl. Phys. Lett.* **2009**, *95*, 063302.
(24) Hau, S. K.; Yip, H. L.; Ma, H.; Jen, A. K. Y. *Appl. Phys. Lett.* **2008**, *93*, 233304.
(25) Hau, S. K.; Yip, H. L.; Jen, A. K. Y. *Polym. Rev.* **2010**, *50*, 474−510.
(26) Liao, H. H.; Chen, L. M.; Xu, Z.; Li, G.; Yang, Y. *Appl. Phys. Lett.* **2008**, *92*, 173303.
(27) Zhang, F. J.; Xu, X. W.; Tang, W. H.; Zhang, J.; Zhuo, Z. L.; Wang, J.; Wang, J.; Xu, Z.; Wang, Y. S. *Sol. Energy Mater. Sol. Cells* **2011**, *95*, 1785−1799.
(28) Yang, J. L.; Schumann, S.; Hatton, R. A.; Jones, T. S. *Org. Electron.* **2010**, *11*, 1399−1402.
(29) Qi, D. C.; Sun, J. T.; Gao, X. Y.; Wang, L.; Chen, S.; Loh, K. P.; Wee, A. T. S. *Langmuir* **2010**, *26*, 165−172.
(30) Yu, X. J.; Wilhelmi, O.; Moser, H. O.; Vidyaraj, S. V.; Gao, X. Y.; Wee, A. T. S.; Nyunt, T.; Qian, H. J.; Zheng, H. W. *J. Electron Spectrosc. Relat. Phenom.* **2005**, *144*, 1031−1034.
(31) Chen, W.; Qi, D. C.; Huang, H.; Gao, X. Y.; Wee, A. T. S. *Adv. Funct. Mater.* **2011**, *21*, 410−424.
(32) Stöhr, J. *NEXAFS Spectroscopy*; Springer-Verlag: Berlin, 1992; Vol. *25*.
(33) Chen, W.; Chen, S.; Huang, H.; Qi, D. C.; Gao, X. Y.; Wee, A. T. S. *Appl. Phys. Lett.* **2008**, *92*, 063308.
(34) Duhm, S.; Heimel, G.; Salzmann, I.; Glowatzki, H.; Johnson, R. L.; Vollmer, A.; Rabe, J. P.; Koch, N. *Nat. Mater.* **2008**, *7*, 326−332.
(35) Fukagawa, H.; Kera, S.; Kataoka, T.; Hosoumi, S.; Watanabe, Y.; Kudo, K.; Ueno, N. *Adv. Mater.* **2007**, *19*, 665−668.
(36) Zahn, D. R. T.; Gavrila, G. N.; Gorgoi, M. *Chem. Phys.* **2006**, *325*, 99−112.
(37) Mao, H. Y.; Bussolotti, F.; Qi, D. C.; Wang, R.; Kera, S.; Ueno, N.; Wee, A. T. S.; Chen, W. *Org. Electron.* **2011**, *12*, 534−540.
(38) Zhu, F.; Wang, H. B.; Song, D.; Lou, K.; Yan, D. H. *Appl. Phys. Lett.* **2008**, *93*, 103308.
(39) Chen, W.; Chen, S.; Huang, Y. L.; Huang, H.; Qi, D. C.; Gao, X. Y.; Ma, J.; Wee, A. T. S. *J. Appl. Phys.* **2009**, *106*, 064910.
(40) Lau, K. M.; Tang, J. X.; Sun, H. Y.; Lee, C. S.; Lee, S. T.; Yan, D. H. *Appl. Phys. Lett.* **2006**, *88*, 173513.
(41) Zhu, F.; Yang, J. B.; Song, D.; Li, C. H.; Yan, D. H. *Appl. Phys. Lett.* **2009**, *94*, 143305.
(42) Yan, X. J.; Wang, J.; Wang, H. B.; Wang, H.; Yan, D. H. *Appl. Phys. Lett.* **2006**, *89*, 053510.
(43) Dai, J.; Jiang, X.; Wang, H.; Yan, D. *Thin Solid Films* **2008**, *516*, 3320−3323.
(44) Wang, J.; Wang, H.; Yan, X.; Huang, H.; Yan, D. *Appl. Phys. Lett.* **2005**, *87*, 093507.
(45) Opitz, A.; Ecker, B.; Wagner, J.; Hinderhofer, A.; Schreiber, F.; Manara, J.; Pflaum, J.; Brütting, W. *Org. Electron.* **2009**, *10*, 1259−1267.
(46) Opitz, A.; Wagner, J.; Brutting, W.; Salzmann, I.; Koch, N.; Manara, J.; Pflaum, J.; Hinderhofer, A.; Schreiber, F. *IEEE J. Sel. Top. Quantum Electron.* **2010**, *16*, 1707−1717.
(47) Lai, S. L.; Chan, M. Y.; Fung, M. K.; Lee, C. S.; Lee, S. T. *J. Appl. Phys.* **2007**, *101*, 014509.
(48) Yu, B.; Zhu, F.; Wang, H. B.; Li, G.; Yan, D. H. *J. Appl. Phys.* **2008**, *104*, 114503.